Quarterly Reviews of Biophysics **33**, 1 (2000), pp. 1–27 Printed in the United Kingdom
© 2000 Cambridge University Press

CCD detectors in high-resolution biological electron microscopy

A. R. Faruqi and Sriram Subramaniam†
MRC Laboratory of Molecular Biology, Hills Road, Cambridge CB2 2QH, UK

1. Introduction 1
1.1 The 'band gap' in silicon 2

2. Principles of CCD detector operation 3
2.1 Direct detection 3
2.2 Electron energy conversion into light 4
2.3 Optical coupling: lens or fibre optics? 6
2.4 Readout speed and comparison with film 8

3. Practical considerations for electron microscopic applications 9
3.1 Sources of noise 9
3.1.1 Dark current noise 9
3.1.2 Readout noise 9
3.1.3 Spurious events due to X-rays or cosmic rays 10
3.2 Efficiency of detection 11
3.3 Spatial resolution and modulation transfer function 12
3.4 Interface to electron microscope 14
3.5 Electron diffraction applications 15

4. Prospects for high-resolution imaging with CCD detectors 18

5. Alternative technologies for electronic detection 23
5.1 Image plates 23
5.2 Hybrid pixel detectors 24

6. References 26

1. Introduction

During the past decade charge-coupled device (CCD) detectors have increasingly become the preferred choice of medium for recording data in the electron microscope. The CCD detector itself can be likened to a new type of television camera with superior properties, which makes

† Present address: Laboratory of Biochemistry, National Cancer Institute, Bethesda, MD 20892, USA E-mail: arf@mrc-lmb.cam.ac.uk *and* ss1@nih.gov

https://doi.org/10.1017/S0033583500003577 Published online by Cambridge University Press

it an ideal detector for recording very low exposure images. The success of CCD detectors for electron microscopy, however, also relies on a number of other factors, which include its fast response, low noise electronics, the ease of interfacing them to the electron microscope, and the improvements in computing that have made possible the storage and processing of large images.

CCD detectors have already begun to be routinely used in a number of important biological applications such as tomography of cellular organelles (reviewed by Baumeister, 1999), where the resolution requirements are relatively modest. However, in most high-resolution microscopic applications, especially where the goal of the microscopy is to obtain structural information at near-atomic resolution, photographic film has continued to remain the medium of choice. With the increasing interest and demand for high-throughput structure determination of important macromolecular assemblies, it is clearly important to have tools for electronic data collection that bypass the slow and tedious process of processing images recorded on photographic film.

In this review, we present an analysis of the potential of CCD-based detectors to fully replace photographic film for high-resolution electron crystallographic applications. We begin with a brief introduction to the principles underlying the operation of CCD detectors. A detailed discussion is then provided of the performance of CCD detectors with respect to efficiency of detection of electrons, accuracy, speed of data storage and retrieval and limits on resolution that can be attained. For each of these performance indicators, we provide an evaluation of the advantages and/or limitations of data recorded on CCD detectors as compared with photographic film for high-resolution microscopic work. Using examples from recently published work, we show that the performance of currently available CCD detectors is already adequate for recording electron diffraction patterns from two-dimensional crystals to resolutions as high as 2 Å. Evaluation of the prospects for routinely using CCD detectors for high-resolution imaging suggests that while further improvements are still required, the outlook for implementing fully electronic data acquisition in the next generation of electron microscopes is excellent.

1.1 The 'band gap' in silicon

The design of CCD detectors relies on the special electrical properties of silicon, a semiconducting material. The regular crystalline structure of silicon forces electrons into two energy bands known as valence and conduction bands, separated by a 'forbidden' energy band gap that is not accessible to electrons associated with the silicon crystal lattice. Electrons in the valence band occupy a range of lower energy states, and are relatively immobile. Electrons with higher energies can jump across the band gap into the conduction band where their association with atoms is no longer very strong and they are therefore free to move, for example, under the influence of a moderate externally applied electrical field. This is especially useful when the electrical properties of 'pure' silicon are altered by adding minute quantities of 'impurity' elements. When subjected to an external source of incident energy, such as visible wavelength photons, some electrons acquire sufficient energy to jump from the valence band into the conduction band, leaving behind the same number of 'holes' in the valence band. The energy originally deposited in silicon is thus mainly converted into electron–hole pairs, which is the basis for photon detection. The signal generated depends on

https://doi.org/10.1017/S0033583500003577 Published online by Cambridge University Press

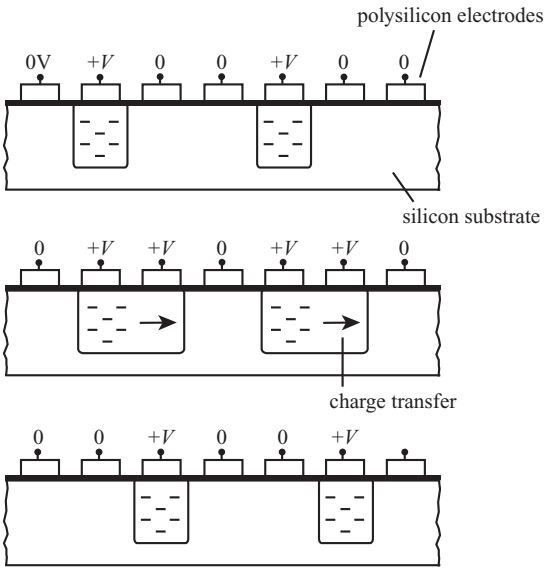


Fig. 1. Schematic diagram showing the process of charge integration and readout in a three-phase CCD. Voltage pulses controlling both integration and readout are applied to the polysilicon electrodes. During integration one of the three phases is kept at a high potential to trap electrons in the potential well formed under the electrode. The readout of charge is accomplished by raising the adjacent pixel also to a positive potential, V. When the original pixel returns to 0 V, the charge is retained in the second pixel, i.e. there is a net flow of charge from one pixel to the next – leading to the term charge coupling. The sequential application of voltage pulses to shift the charge is known as 'clocking'.

the properties of silicon: the energy of the band gap for silicon is 1·12 eV (electronvolts), and the energy required to produce an electron–hole pair 3·55 eV.

The key feature that allows silicon to be converted into a position sensitive detector or an imaging device, is that it can be divided into a large number of independent picture elements or pixels. Electrons formed due to light falling on one pixel are confined to that pixel, by electric fields, until the image recording is completed. The readout of this stored charge from the CCD relies on a remarkable property of charge coupling between adjacent pixels (Fig. 1). Charge is shifted along the row, from pixel to pixel, until it reaches an output 'sense' node, where it is measured in a charge-sensitive amplifier. When the pixels from an entire row have been read out the adjacent row is shifted into the first row and all the pixels from the row are read out. The procedure is repeated until all rows, i.e. the entire image has been read out.

2. Principles of CCD detector operation

2.1 Direct detection

CCD detectors are sensitive to many sources of incident radiation, including visible photons, X-rays or electrons that can create a sufficient number of electron–hole pairs. Since the energy required to create an electron–hole pair in silicon is 3·55 eV, the energy deposited by electrons used under standard imaging conditions in electron microscope (100 keV or greater) is more than adequate to produce a reasonably high signal.

https://doi.org/10.1017/S0033583500003577 Published online by Cambridge University Press

However, direct detection of electrons is not yet a practical option for most applications. First, the signal generated by an electron with an energy of even 100 keV is so large that it would fill a substantial proportion of the pixel well capacity (assuming all the energy is deposited in a single pixel) and reduce the dynamic range of the measurements to unacceptably low levels. This argument is not valid when using the silicon device as a 'photon' counter as in hybrid pixel detectors (discussed in Section 5.2), which record a single count per incident electron rather than store the charge in an analog form as in CCD detectors. Second, there would be unacceptably high levels of radiation damage due to the energy deposited by the electrons in the front surface, which contains the polysilicon gates used for applying voltages needed for the readout process. Studies of the damage to CCD detectors by photons of various energies and gamma rays suggest that the charge transfer efficiency is degraded, and would result in a useful life of only a few hours owing to charge trapping in the interface between silicon and silicon dioxide (Roberts *et al*. 1982). Back-side illuminated CCD detectors may have somewhat less radiation damage as the polysilicon gates are on the reverse side, i.e. the electrons would first need to travel through the bulk silicon before encountering the gates, but the extent of damage would still be too high from electrons which traverse the CCD thickness. Third, a number of X-ray quanta that originate further up in the microscope column would be recorded as very high (and spurious) count events in the CCD. This problem is greatly reduced in CCD detectors that use phosphors which convert the incident energy of the electrons into photons (see next section), since most X-ray photons are absorbed by the fibre optics assembly (which couples the phosphor to the CCD).

2.2 Electron energy conversion into light

Most CCD cameras used in electron microscopy rely on recording a very low light level image, formed by visible wavelength photons, when the incident electrons impinge on a special scintillating screen. The screen can either be a free-standing single crystal or a polycrystalline fine grain phosphor. The light image formed on the scintillator is imaged on to the CCD detector either with lens coupling or with fibre optics. The scintillator (i.e. phosphor) forms a crucial component, as it forms the low light level image, which is subsequently imaged by the CCD detector. A list of 'desirable' properties of the phosphor would include the following:

- high conversion efficiency into visible radiation,
- reasonably short and well-defined decay time of the emitted scintillation,
- phosphor output wavelength matched to CCD sensitivity (which has a maximum at ~ 700 nm),
- resistance to radiation damage,
- a convenient, reproducible method of depositing a thin layer of phosphor on a flat surface.

A number of polycrystalline phosphors are available which match some of the required properties listed above. Much of the earlier work in electron imaging was carried out with yttrium aluminium garnet (YAG), a single crystal scintillator (Autrata *et al*. 1983). A major drawback of using YAG in a CCD detector is that the scintillator is only available in limited sizes of up to ~ 40 mm diameter. The conversion efficiency for YAG is also lower than for

https://doi.org/10.1017/S0033583500003577 Published online by Cambridge University Press

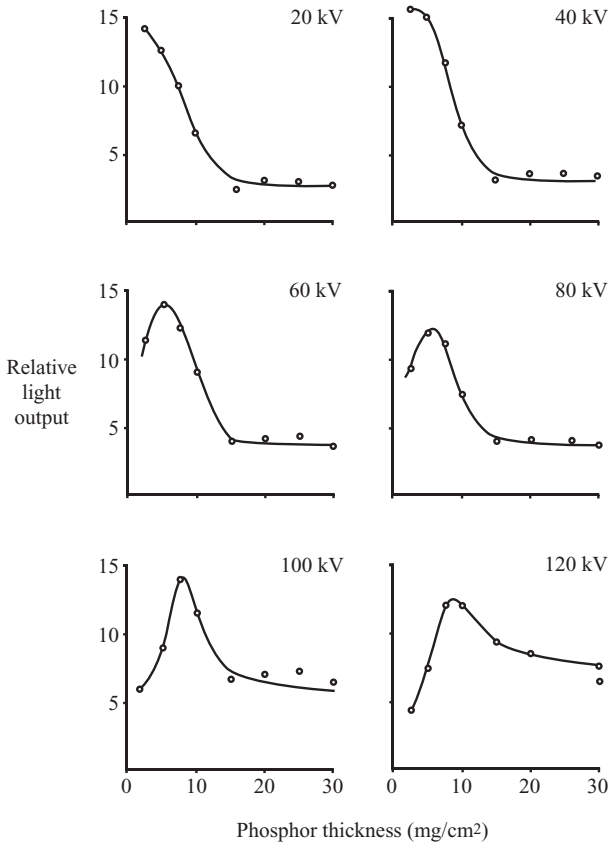


Fig. 2. Relative light output in P43 phosphor; light output is shown as a function of phosphor thickness for a range of incident electron energies. The peak of emission shifts to greater coating thickness for higher energies. The coating thickness is represented in units of surface density (mg/cm^2) of the deposited layer of phosphor.

the polycrystalline phosphors discussed below (Daberkow *et al*. 1996). In recent years, YAG has been largely replaced by two phosphors that can be obtained in larger sizes: P20, which is zinc cadmium sulphide doped with silver, and P43, which is gadolinium oxy-sulphide doped with terbium (Faruqi *et al*. 1995). Both have higher conversion efficiencies than YAG, but P20 has a rather long and intensity-dependent decay time-constant, which makes it less attractive than P43.

P43 has particularly attractive properties for electron imaging with a high conversion efficiency of 12–20 %, and produces an excellent signal from 120 keV electrons (Faruqi *et al*. 1995). The decay constant of light emitted by the phosphor is reasonably short, taking $\sim$ 3 ms for decay to the 1 % level. This is adequate for most applications, since the time taken for readout of the signal, which may be several seconds, is usually the rate-limiting step. Most of the light emitted from the phosphor is at a wavelength of $\sim$ 550 nm, which is not ideal for CCD detectors, which have a peak efficiency for detection at $\sim$ 700 nm. However, the quantum efficiency at 550 nm is $\sim$ 25 %, which is still sufficiently high. The P43 phosphor also has excellent radiation resistance, as there is little sign of damage in phosphors that have been used for periods of over 2 years (Faruqi & Andrews, 1997).

https://doi.org/10.1017/S0033583500003577 Published online by Cambridge University Press

For a given type of phosphor, it is important to make a careful choice of the coating thickness to obtain the maximum signal. The optimal thickness depends on the incident electron energy. Comparisons of light output for different thicknesses are described by Fan & Ellisman (1997) for the P20 phosphor and by Faruqi & Tyrell (1999) for the P43 phosphor. In general, the resolution obtained from a given phosphor is better for thinner phosphors as there is less light scattering within the phosphor grains. However, at very small thicknesses, there is a loss of light due to inadequate absorption of the electron energy. The optimal thickness is therefore a compromise between these two features. Measurements on light output due to electrons of 20–120 keV, as a function of phosphor coating density are shown in Fig. 2. At higher energies (> 60 kV) light output is low at small densities, increases to a maximum and then decays for greater densities, owing to self-absorption and multiple light scattering in the phosphor. The optimum density for 120 kV electrons has been determined to be ~ 10 mg/cm^2 which corresponds to an approximate thickness of 40 μm (Faruqi & Tyrell, 1999). For energies greater than 120 keV, Fan & Ellisman (1997) also found a near-monotonic increase in light output with the thickness of the (P20) phosphor; at 250 keV, the optimal thickness was measured as being 55–60 μm.

2.3 Optical coupling: lens or fibre optics?

The 'light' image made by the high-energy electrons on the phosphor needs to be imaged, via suitable optics, on to the CCD detector. Imaging can be done either with a lens or a fibre optics assembly. The main advantage of lens coupling is that it is somewhat simpler to get rid of spurious 'noise' signals due to secondary X-rays (but not cosmic rays). Because X-rays are emitted radially from the specimen it is preferable to remove the CCD detector from the direct path by bending the optical path, as implemented by Fan & Ellisman (1993) and shown in Fig. 3(*a*). In this arrangement, the phosphor, an 'extended' P20, is deposited on a leaded glass window, the latter acting as a vacuum/radiation shield. A two-lens system images the phosphor plane on to the CCD detector with a 90° bend in a prism. Since the CCD detector is not located in the microscope vacuum it is simpler to access the associated electronics and other components and the lenses can be exchanged to alter magnification in the optics.

A second approach to optical coupling is to use well-established coherent fibre optics technology, developed specifically for transmitting images (Daberkow *et al*. 1991; Kujawa & Krahl, 1992; Krivanek & Mooney, 1993; Faruqi *et al*. 1995). A bundle of 'coherent' optical fibres is a very efficient method of transmitting an optical image from the phosphor onto the CCD detector. The fibre optics coupler consists of a large number of very fine (typically 5–10 μm diameter) glass fibres, coated with a higher refractive index glass, and fused to form a bundle. The extremely high light transmission in the fibre optical bundle results from the high efficiency of total internal reflection of optical rays (total internal reflection coefficient $> 0{\cdot}9999$ as compared to an efficiency of $\sim 0{\cdot}95$ for simple reflection from a polished metal surface). Optical fibres within a bundle are precisely aligned so that the image projected on one side of the bundle stays coherent on the output side. Light spreading across fibres is minimized by inserting 'dark' absorbing fibres (called extra-mural absorbers), which restrict optical cross-talk between pixels. It is also possible to alter the magnification of the transmitted image by introducing a taper in the bundle, by varying the diameter between input and output ends. De-magnification factors of up to approximately three are routinely used in imaging systems but values beyond four produce technical problems (Coleman, 1985).

https://doi.org/10.1017/S0033583500003577 Published online by Cambridge University Press

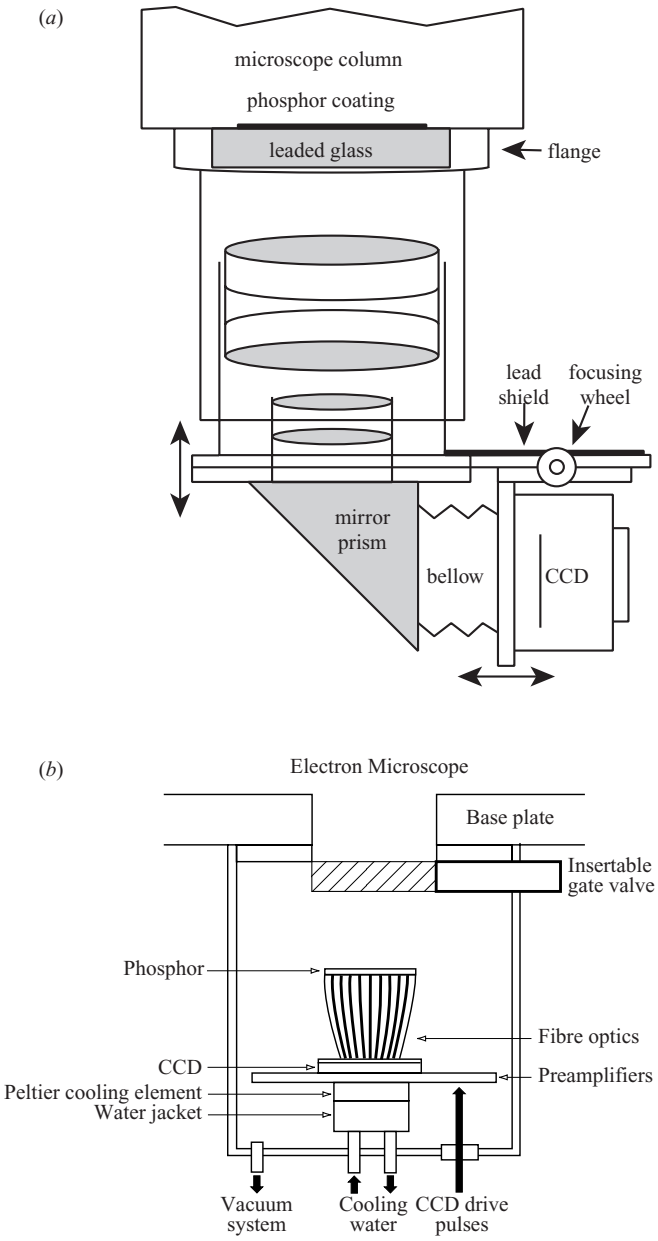


Fig. 3. (*a*) CCD Detector with lens coupling, from Fan & Ellisman (1993). The phosphor (P20, 20 μm thickness) coating is deposited on a special lead glass, which also isolates the microscope vacuum. The light path is bent through 90° in the prism to reduce problems of spurious signals due to X-ray photons. (*b*) CCD detector with tapered fibre optics, from Faruqi & Andrews (1997). The phosphor (10 mg/cm² of P43) is directly deposited on the larger face of a tapered fibre optics assembly, which has a demagnification of 1·7. A gate valve is used to isolate the detector from the microscope vacuum.

The principal advantage of fibre optics coupling lies in the amount of light transmitted compared to lens coupling. Even for the optical case of 1:1 lens coupling, the fibre optics transmission is higher but the difference becomes more significant at higher demagnification

https://doi.org/10.1017/S0033583500003577 Published online by Cambridge University Press

values (Coleman, 1985). For example, at a demagnification of 2·5:1, the fibre optics transmits ~ 10 times more light than a lens-coupled system. The optical alignment of fibre optics is much simpler as no focusing is involved. Fibre optics detector assemblies are more stable and robust as all parts are fixed rigidly. A potential disadvantage of tapered fibre optics is that some distortion is usually introduced in the manufacturing process, which involves heating and stretching bundles of fibres. The distortion figures at the edge of the aperture are typically 2–3%. However, this distortion can be computationally corrected after data acquisition (see Section 3.5). A schematic illustrating the design of a CCD detector with tapered fibre optics, interfaced to a CM-12 electron microscope is shown in Fig. 3(*b*). In this design (Faruqi & Andrews, 1997), the P43 phosphor is deposited directly on the front face of the fibre optics assembly, which is optically coupled at the far end to the CCD detector. Larger sensitive areas can be obtained by tiling CCD detectors into a 2 × 2 array and using a larger demagnification in the tapered fibre optics. Faruqi *et al*. (2000) have reported construction of a detector with a sensitive area of 140 mm × 130 mm with 2500 × 2300, 56 μm square pixels at the phosphor.

2.4 Readout speed and comparison with film

The main functions of the CCD detector control electronics during imaging are to set up the appropriate voltages on the gates to allow the image to be integrated during the exposure part of a cycle and to read out and measure the accumulated charge signal from the individual pixels at the end of the exposure. The readout of the image from the CCD detector requires a preset sequence of clock pulses depending on the number of phases in the CCD (commonly three-phase), the number of pixels per row and the number of columns (Mclean, 1989). CCD manufacturers usually give guidelines regarding the size and shape of the clock pulses, which vary from one device to another. Once the charge has been transferred to the output sense node of the CCD, the measurement of this charge is a much more delicate operation (than clocking) requiring special low-noise circuits, which amplify the signal and minimize the noise. At the output stage, the charge on the pixel being read out is transferred to a capacitor, which develops a voltage V given by:

$$V = Q/C$$

where Q is the charge deposited by the pixel and C is the capacitance. Very low noise readout can be achieved if correlated double sampling (CDS) mode of readout is employed; in this method the voltage developed on the capacitance is measured prior to, and after, being charged. The CDS method gives a much more accurate value than a single measurement, as it eliminates any variations in the reset voltage (i.e. zero level) of the capacitance. It is possible to achieve relatively low values of readout noise (~ 10 e^- rms) with readout times of ~ 10 μs/pixel and 30 e^- rms with ~ 1 μs/pixel (Faruqi *et al*. 1995). The CDS circuit is usually followed by a suitable amplifier and a fast analog-to-digital converter, which converts the charge to 12 bits (maximum 4096 counts) or 16 bits (maximum 65 535 counts) resolution. The digitized values of the pixel charge are stored in a random access memory or magnetic disk for further analysis. For a 1 million pixel CCD detector with two readout channels, it is thus possible to complete the image readout, with the lower noise readout, in about 5 s; with faster and 'noisier' readout the time is reduced to ~ 1 s. The speed of readout in CCD detectors is one of the principal advantages over film; one avoids all manual aspects of film developing

https://doi.org/10.1017/S0033583500003577 Published online by Cambridge University Press

and digitizing (both of which can be lengthy and tedious procedures), as well as artifacts from day-to-day variations in the strength of the developer or scratch marks on the emulsion.

3. Practical considerations for electron microscopic applications

3.1 Sources of noise

There are three main sources of noise in CCD images: dark current noise, readout noise, and spurious events due to X-rays or cosmic rays. For images recorded on film, the first two sources are of course not relevant, and contributions from X-rays or cosmic rays are generally not very serious. However, each of these sources of noise can degrade a CCD image, and it is therefore important to consider them in more detail.

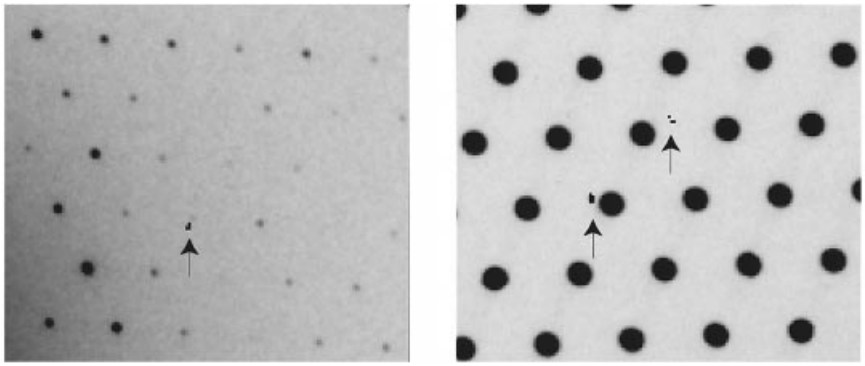
3.1.1 Dark current noise

Electrons in the silicon crystal lattice possess thermal energy, which allows them occasionally to jump spontaneously across the band gap into the conduction band, where they become 'free' electrons. The generation of free electrons without any illumination falling on the CCD detector results in a 'dark' image, which needs to be subtracted from an acquired image. Dark current generation is strongly temperature dependent; there is an approximately two-fold reduction in dark current for every 6–8 °C reduction in temperature. At room temperature, the dark current is sufficiently large to fill pixel wells to full capacity in only a few seconds, making the device virtually useless for low light level imaging. The exposure times normally required in electron microscopy are usually well under 60 s for which the dark current can be reduced to acceptably low levels by cooling the CCD detector to ~ -30 °C by thermo-electric cooling devices. Although dark current can be easily subtracted from a recorded image, the shot noise in the dark current adds a small uncertainty in the measured values indicating that dark current should be minimized for highest accuracy. It is possible to obtain specially designed CCD detectors, which have considerably reduced dark current, known as multi-pinned phase devices (MPP), though the pixel well capacity and consequently the dynamic range is also reduced in these devices (EEV, UK, Technical Data Sheets).

3.1.2 Readout noise

Because of the low readout noise levels, it is possible to obtain a signal from only a small number of electrons incident on a pixel. The readout noise can be put in perspective by calculating the approximate size of signal delivered by a single visible light photon. As mentioned earlier, the quantum efficiency of silicon at a wavelength of 550 nm is $\sim 0{\cdot}25$, i.e. one would get one free electron for about four incident light photons. The lowest attained noise figures in commercially obtained CCD detectors are $\sim 2\ e^-$, resulting in a S/N for single photon detection of $\sim 0{\cdot}1$. The situation is somewhat different for recording, say, 120 keV electrons, as there is more energy deposited and more light available, but it is nevertheless important to keep the signal-to-noise figure as high as possible for efficient detection. Readout noise of 2–5 e^- rms, can usually be obtained only with a relatively slow readout rate of ~ 20 μs/pixel. When signal-to-noise ratio is not critical then a higher value of readout noise

https://doi.org/10.1017/S0033583500003577 Published online by Cambridge University Press



(*a*) (*b*)

Fig. 4. Two examples of 'spurious' events recorded by the CCD due to cosmic rays or X-rays. (*a*) Region from a diffraction pattern obtained with bacteriorhodopsin crystals that include a sharp, intense spot shown by an arrow, probably arising from a cosmic ray event recorded in the CCD. (*b*) A similar record of cosmic rays in a spot-scan image. The exposure time for a spot-scan image is 65 s (compared to only 10 s for the diffraction pattern) and the cosmic ray and X-ray events occur with a correspondingly higher frequency.

can be tolerated with a faster readout (as mentioned above), such as provided by a clamp-and-sample technique which can operate at a readout rate of 1 μs/pixel with 30 e^- noise (Faruqi *et al*. 1994). Further gains in readout speeds can be made by employing more than one readout node on the CCD. Some commercially available devices have up to four outputs, although at a higher cost.

3.1.3 Spurious events due to X-rays or cosmic rays

As discussed in Section 2.1, CCD detectors are also sensitive to other types of radiation besides electrons and visible photons, which have the detrimental effect of generating unwanted 'spurious' background-type events when used in the electron microscope. Common sources that generate spurious signals include:

- radioactive decay from elements used in the construction of the detector, e.g. trace elements of thorium used in the manufacture of fibre optics,
- high-energy cosmic ray particles traversing the CCD,
- X-ray photons created by electron bombardment of material in the microscope column, the number and energy of the X-ray photons being dependent on the electron energy used in the microscope.

The contribution from these events increases with size of the pixel array. As discussed later, it is possible in some cases to make corrections for the noise introduced by such spurious signals.

The signals produced by high-energy cosmic rays are very highly localized as the particles leave a trail of electron–hole pairs in the sensitive region of the CCD. Typically, the sensitive depth region in the CCD detector used normally for low light level imaging is ~ 10 μm (EEV UK, Technical Notes) and an energetic particle deposits sufficient energy to create > 1000 electrons, usually spread over just one or two pixels. This large number of localized electrons produces a characteristic 'spike' in the image (Fig. 4(*a*)), which can be removed with the aid

https://doi.org/10.1017/S0033583500003577 Published online by Cambridge University Press

of a software algorithm that ignores pixels with values very much higher than other pixels in the vicinity.

In fibre optic coupled CCD detectors, much of the stray X-ray photons generated in the column are attenuated by the fibre optics assembly. However, X-ray photons can also be detected in the phosphor where their energy is converted to light. This conversion, however, occurs with much poorer efficiency as the phosphors are thinner than would be required for efficient X-ray detection. For imaging applications, it is therefore difficult to distinguish the spurious signal due to these X-ray photon conversions from the real signal that originates from electrons incident on the phosphor. However, for electron diffraction applications, this is not a serious problem because the majority of these spurious signals are not located where the diffraction spots occur (Fig. 4(*b*)), and are not included for extracting spot intensities.

The contribution of cosmic and X-ray events to the dark background signal can be effectively corrected. Since both cosmic and X-ray events are random and generally affect only a small fraction of pixels ($< 1\%$) in a given exposure period, a series of images can be recorded and an image can be constructed by simply using the minimum value recorded in a given pixel. A more sophisticated correction to get a more accurate estimate of the background noise in a given pixel could be based on calculation of the variance over many measurements, rejecting outlier values, and averaging the rest.

3.2 Efficiency of detection

CCD detectors belong to a class of detector in which the signal (i.e. the image being recorded) is integrated as a charge in the pixel wells during the exposure period. The image is read out at the end of the exposure. Detectors belonging to this category, which include film, vidicons and phosphor imaging plates, are most commonly employed in electron microscopy. The other main category of detectors rely on 'counting' individual quanta and include multiwire gas-based detectors, silicon pixel detectors, etc. (Faruqi, 1991). Characterization of detectors, i.e. a description of the key properties of the detector, is an important consideration for judging the usefulness of a particular detector system for a given application. Among the important properties of the detector are: accuracy of measurements possible (including signal degradation due to added noise by the detector), spatial resolution (or modulation transfer function) and miscellaneous detector artifacts including spurious events due to cosmic rays, background X-rays or some other source. This discussion is focused on CCD detectors, although some of the general concepts are equally applicable to other detectors.

One of the most important properties of the detector is the efficiency with which it can detect electrons. Because the detection and readout process also contains noise from a number of different sources, e.g. readout noise or shot noise, a useful definition of efficiency is the 'detective quantum efficiency' (DQE), which takes into account the noise in the detection process.

$$\mathrm{DQE} = \frac{(\mathrm{signal}/\mathrm{noise})_{\mathrm{output}}}{(\mathrm{signal}/\mathrm{noise})_{\mathrm{input}}}$$

If the noise contributions were only from 'shot' noise, as is the case in a 'digital' detector, then the DQE would be simple to calculate. Thus if 100 electrons were incident on the detector and 90 detected, the DQE would be 0·9. If additional noise is being added by the detector, as it usually is in an integrating detector, DQE is less than that calculated on the

https://doi.org/10.1017/S0033583500003577 Published online by Cambridge University Press

basis of the 'shot' noise alone. In the more general case, the number of photons emitted by the phosphor per incident electron is given by:

$$n_{\mathrm{ph1}} = (E/h\nu)^{*}\epsilon_{\mathrm{ph}}$$

where

n_{ph1} = number of light photons emitted over 4 π
E = energy of incident electron (in eV)
$h\nu$ = energy of light photon (in eV)
ϵ_{ph} = efficiency of energy conversion in the phosphor.

Only a small fraction of the emitted photons will be accepted by the fibre optics and there is a further attenuation of light in the fibre optics. The number of photons which fall on the CCD, n_{ph2}, are given by:

$$n_{\mathrm{ph2}} = n_{\mathrm{ph1}}{}^{*}\epsilon_{\mathrm{optics}}$$

where $\epsilon_{\mathrm{optics}}$ = light collection efficiency of the optics. The number of electron–hole pairs generated by the incident photons, given by n_{pe}, is:

$$n_{\mathrm{pe}} = n_{\mathrm{ph2}}{}^{*}\epsilon_{\mathrm{qe}}$$

where ϵ_{qe} = quantum efficiency of silicon.

The value of the various parameters used in the calculation of n_{pe} is discussed in greater detail elsewhere (Faruqi *et al*. 1999). A rough estimate is provided below by using simplified assumptions. Assuming that the incident electron has an energy of 120 keV (and deposits all that energy in the phosphor), a value of 0·12 for the energy conversion efficiency of the phosphor, a value of 0·5 for the fraction of light collected by the fibre, transmission efficiency of 0·1 for the fibre optics assemblies and a value of 0·25 for the quantum efficiency of the CCD, and assuming that the energy of the emitted light photon is 2·2 eV, we obtain a value for the output signal from the CCD of

$$n_{pe} = (120\,000/2{\cdot}2)^{*}0{\cdot}12^{*}0{\cdot}5^{*}0{\cdot}1^{*}0{\cdot}25 = 80$$

In the event that all the photons are deposited on a single pixel, this is an excellent signal for a typical slow-scan readout CCD. The problem with most CCD detectors is that because of the spread of emitted light photons in the phosphor, the signal is spread over many pixels. If the signal is spread over 10 pixels, the value per pixel is then approximately eight electron–hole pairs, which is of the same magnitude as the readout noise. The aim of CCD detector design is to optimise each of the steps in the signal transmission process to obtain the most efficient detection system. The efficiency of CCD detectors is compared with film in Section 3.5 for diffraction work. It is shown that CCD detectors have superior efficiency for recording weaker diffraction spots, owing partly to the lack of 'fog' that is present in film images.

3.3 Spatial resolution and modulation transfer function

Resolution is an important concept in any imaging system. A measure of resolution in an electron microscopic image recorded by a CCD detector is given by the so-called 'point spread function', which defines the response of the detector to a 'point' source of electrons.

https://doi.org/10.1017/S0033583500003577 Published online by Cambridge University Press

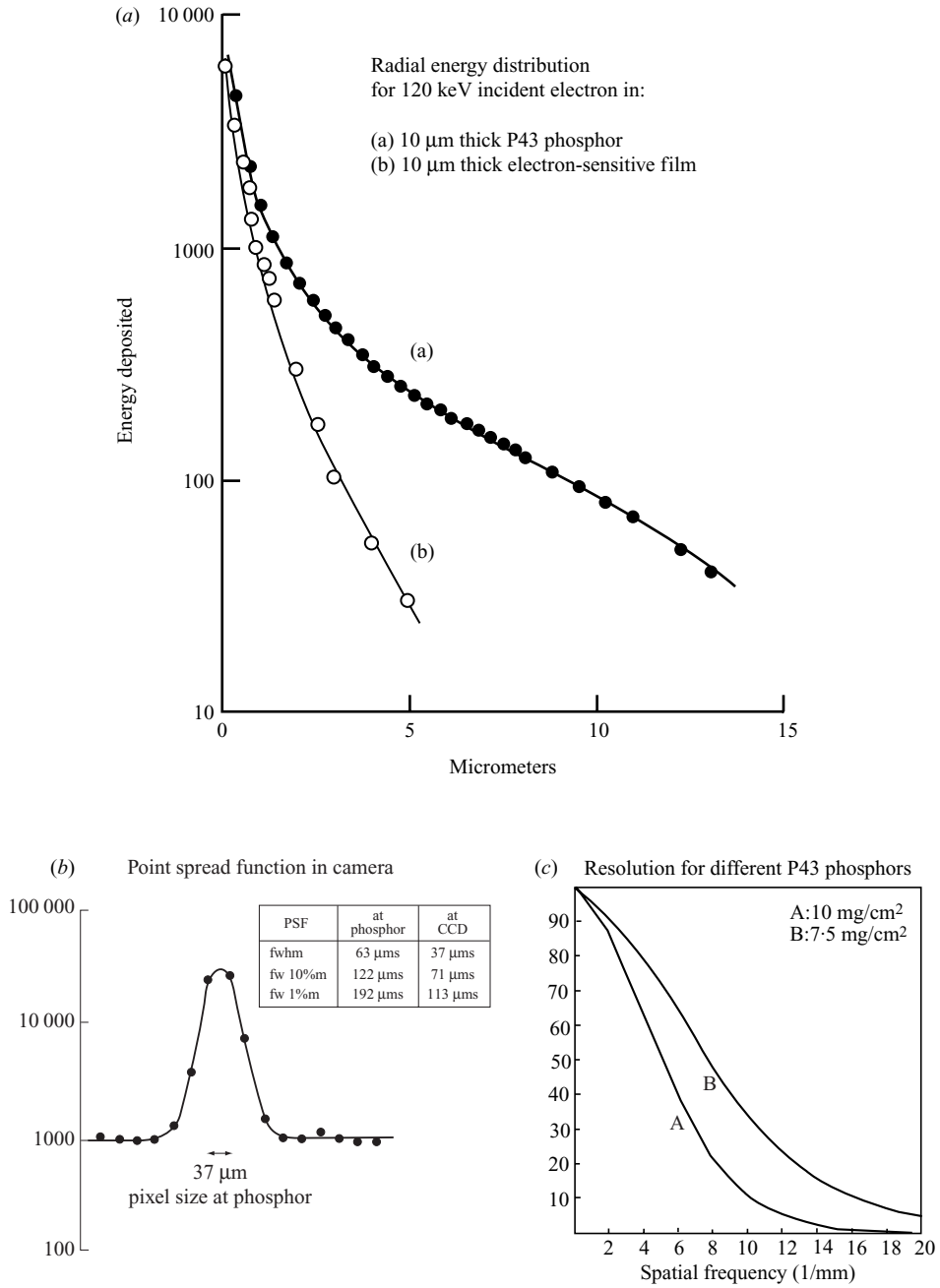


Fig. 5. (*a*) Monte Carlo simulations used to estimate the expected spread of energy from 120 keV electrons incident on 10 μm thick electron-sensitive film or P43 phosphor. (*b*) Experimental measurement of point spread function in a detector with P43 phosphor-coated fibre optics. Measurements were made with 120 keV electrons. (*c*) Modulation transfer function for two coating densities of P43 at 120 keV.

Monte Carlo simulations (Faruqi & Andrews, 1997) to estimate the degree of electron scattering in the phosphor shown in Fig. 5(*a*), suggest that the point spread function (PSF) is ~ 20 μm, full width at 1% maximum (see also Daberkow *et al.* 1991; de Ruijter & Weiss,

https://doi.org/10.1017/S0033583500003577 Published online by Cambridge University Press

1992; Daberkow *et al*. 1996; Meyer & Kirkland, 1998). A similar exercise for film suggests an even smaller PSF of 10 μm width (full width at 1% maximum). An experimental measurement of the PSF, shown in Fig. 5(*b*), describes the spatial spread expected for illumination with a point source of electrons incident on the phosphor. The measured PSF is more than an order of magnitude greater than expected from purely electron scattering considerations suggesting that the major part of the degradation in resolution arises from multiple light scattering within the phosphor. Some measurements on resolution are also available at higher energies; for example, Daberkow *et al*. (1991) found that the PSF in a YAG scintillator (thickness: 50 μm) increased from 62 μm to 84 μm (full width at half maximum) when the incident electron energy was increased from 100 to 300 keV. Resolution measurements at various thickness of the P20 phosphor (range: 12–57 μm) were made by Fan & Ellisman (1997) and a direct correlation was found between greater thickness and poor resolution. However, as the efficiency is lower for thinner phosphors, a compromise has to be made between resolution and efficiency.

The Fourier transform of the point spread function is the modulation transfer function (MTF) which essentially describes how the camera attenuates different spatial frequencies present in the input signal (Fig. 5(*c*)). Thus, for a given input signal, the output image is simply the convolution of the input signal with the point spread function. For high-resolution imaging the consequence is that while features of the image with low spatial frequencies are recorded faithfully, features with higher spatial frequencies are progressively attenuated by the detector. Depending on the resolution of the detector, a cut-off frequency is reached when the transmission drops to zero. The limiting resolution for a given CCD depends directly on the size of the pixel, and can be no higher than the Nyquist frequency, $1/(2*d)$, where d is the linear dimension of the pixel. Theoretical considerations indicate a maximum possible transmission of 63% of the input signal at this limiting frequency. However, this limiting resolution may not be achieved depending on the MTF of other components employed in the detection, each of which will have its own characteristic MTF that modifies the signal. In almost all phosphor-based CCD cameras currently used for electron microscopic applications, the largest contribution to loss of resolution at higher spatial frequencies is from the spread of the emitted light photons in the phosphor layer.

3.4 Interface to electron microscope

The installation of a CCD detector in the electron microscope is an important and critical aspect for optimal performance. One of the main problems is that it is not possible to have the detector, or at least the entrance to the detector (i.e. the scintillator), separated from the high vacuum in the microscope. The most commonly adopted solution is to enclose the camera in a vacuum housing and attach it with a vacuum seal to the microscope (Faruqi *et al*. 1995). The 'integral' scheme has the advantage that a more efficient form of light coupling with fibre optics can be used instead of lens coupling. Lens coupling is really the only choice when a scintillator is placed within the vacuum and imaged through a plate glass on to the CCD outside the vacuum (Fan & Ellisman, 1993; Faruqi *et al*. 1994). Whichever method of attachment is used, it is most important to be able to achieve a good vacuum in the microscope to prevent contamination of the specimen, as this degrades resolution. Further, to maintain high resolution it is essential to reduce the amount of additional mechanical

https://doi.org/10.1017/S0033583500003577 Published online by Cambridge University Press

vibrations introduced through the camera. One source of vibration is from an additional vacuum pump, attached to evacuate the camera, without mechanical de-coupling. Another source of mechanical vibration is a water pump to re-circulate cooling water needed to extract heat from the Peltier thermo-electric cooling devices. The solution adopted for both these potential problems has been to utilize the vacuum pumps already installed on the microscope and to use a small fraction of the gravity-fed cooling water used in the microscope to remove heat from the Peltier device (Faruqi *et al*. 1994).

During usage of film in the microscope it is important to isolate the camera. One solution (Faruqi *et al*. 1995) is to mount the camera with an insertable gate valve, which allows CCD exposures when it is open and film exposures when it is closed. An additional benefit of using the gate valve is that it is possible to remove the CCD camera for servicing with the gate valve closed. It is also important to co-ordinate illumination of the specimen with the electron beam so that it is exposed only during the 'exposure period' (and not before). The CCD detector cannot be illuminated immediately after the exposure period when the charge is being read out to prevent 'smearing' of the recorded image. The required beam controls can be accomplished with control electronics that apply a displacement to the electron beam upon receiving a signal to accumulate a new image. The beam is thus 'blanked', allowing time for clearing out any previously accumulated charge from the CCD. Similarly, a displacement applied at the end of the exposure for the readout period ensures that the image is read out without extra illumination.

3.5 Electron diffraction applications

The most successful use of CCD detectors in high-resolution biological electron microscopy so far has been the acquisition of electron diffraction patterns from two-dimensional crystals of proteins (Brink & Tam, 1996; Mitsuoka *et al*. 1999; Downing & Hendrickson, 1999; Faruqi *et al*. 1999). CCD detectors have several important advantages over film for recording electron diffraction patterns. They have a dynamic range that is 2 orders of magnitude greater than film for recording intensities. The range of intensities in a diffraction pattern from a two-dimensional protein crystal such as bacteriorhodopsin varies from about 2×10^{-5} of the intensity of the undiffracted beam for the strongest spot to about 2×10^{-8} for some of the weakest spots at high resolution. Thus, the entire range can be captured in a single exposure. For most applications, it is relatively easy to identify conditions where the width of the spots is sufficiently small compared to the spacing between spots even for a 1 K × 1 K CCD camera. Further, adequate signal-to-noise ratios can be obtained with doses that are about ten times lower than those required for obtaining comparable signal-to-noise ratios on film.

Accurate measurement of diffraction intensities with a CCD camera requires that any distortions introduced by the fiber optic coupling can be effectively corrected. This is especially relevant if tapered fiber optics are used, since there can be significant distortions introduced by the taper at the edges of the bundle. For automated measurement, it is also important that the measuring program is able to predict the position of the spots accurately. Computational procedures have been developed to deal with both of these issues (Faruqi *et al*. 1999), and are briefly reviewed below.

Predictions for approximate spot locations are based on a calculated lattice using standard methods (Baldwin & Henderson, 1984) using lattice vectors derived from strong spots near the center of the pattern. A general method for correcting distortions has been used which

https://doi.org/10.1017/S0033583500003577 Published online by Cambridge University Press

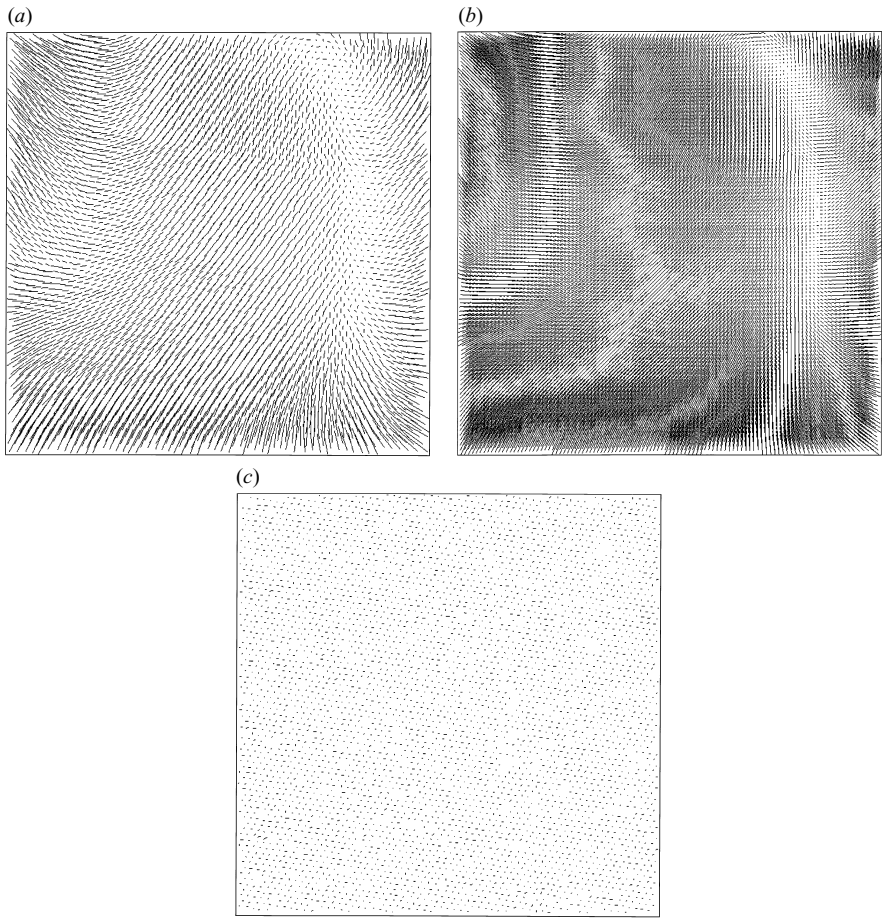
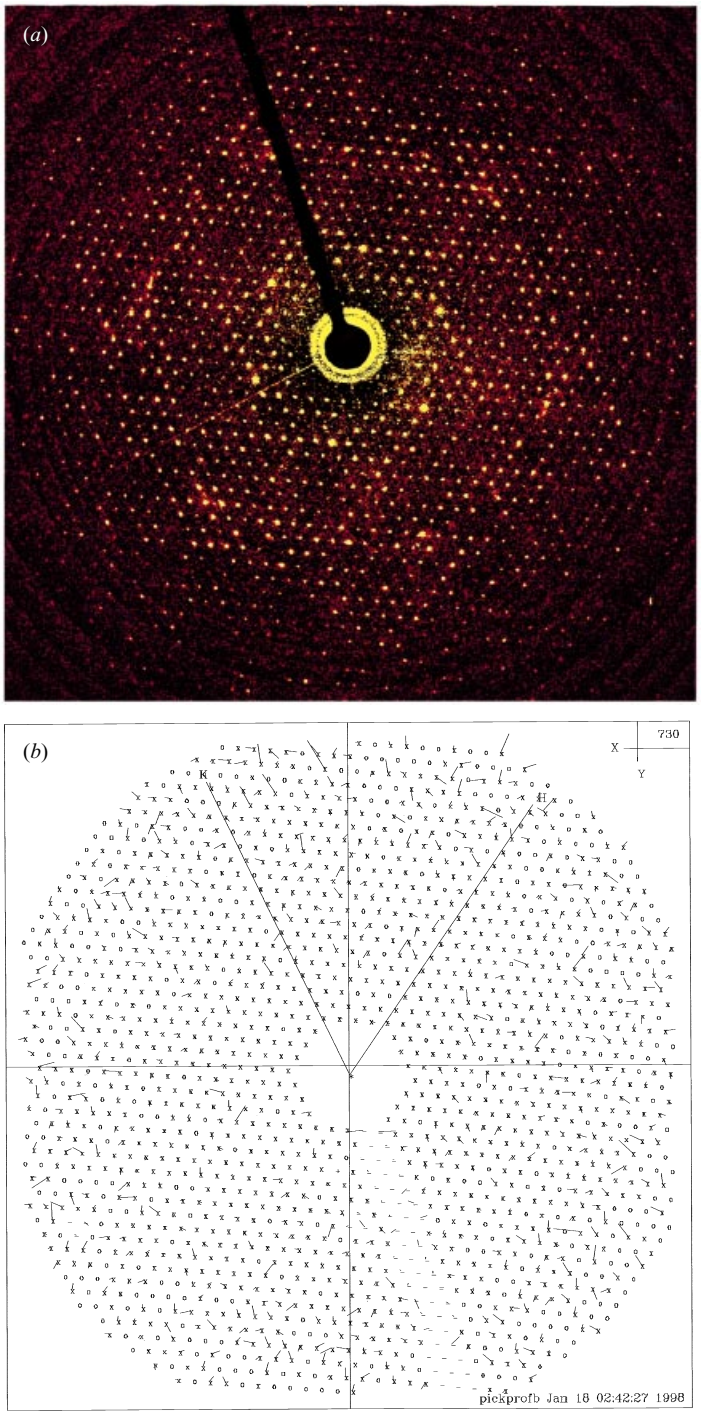


Fig. 6. (*a*) Distortion vectors, magnified 10-fold for improved visibility, representing the spatial distortions in the tapered fibre optics. (*b*) Distortion vectors as in (*a*) but after smoothing and interpolation to a finer grid. (*c*) Residual distortion vectors after computational correction.

is based on generating an array of spots on a well-defined and precise lattice using a spot-scan generator (Tews, 1996). The lattice parameters are measured by using the central part of the sensitive area of the phosphor, where distortions are minimal. The centroids of the complete matrix of spots is then measured and compared with the 'expected' value, the difference between the two representing the deviation due to distortions. The distortion vectors for each lattice point is measured and, after smoothing, recorded in a correction table, which is used to shift the expected position of real diffraction spots. The three steps in the scheme are illustrated in Fig. 6. Fig. 6 (*a*) shows the distortion vectors in the camera, magnified by 10 for better visibility. Smoothing (by applying a bi-cubic spline using 10 evenly spaced knots) allows interpolation on a finer scale shown in Fig. 6 (*b*). Once the corrections have been applied, the residual distortion is reduced to an acceptably small level, shown in Fig. 6 (*c*).

Fig. 7. *Opposite*. (*a*) A diffraction pattern (duration 7 s) from bacteriorhodopsin with the radial background subtracted. A backstop (which casts a shadow of ~ 2·8 mm in the phosphor plane), held in place by a fine wire (which appears to be ~ 0·75 mm thick in the phosphor plane), is used to prevent the direct beam from overloading the central pixels and the shadow from the wire is seen in the lower part of the

https://doi.org/10.1017/S0033583500003577 Published online by Cambridge University Press



pattern. Spots are visible out to ~ 2 Å^{-1} resolution. (*b*) A summary of the spots shown in (*a*); underloads are indicated by a $-$sign, overloads by a $+$sign and 0 denotes a spot measured but not detected above a certain threshold. A cross (X) indicates spot detection and measurement of centre of gravity, with a plot of the deviation from the refined lattice indicated by a vector whose length is $10\times$ the actual deviation in position of the centre of gravity.

https://doi.org/10.1017/S0033583500003577 Published online by Cambridge University Press

One way to assess the effectiveness of these corrections and the accuracy of the recorded data is to estimate differences in intensities for symmetry related reflections (Friedel pairs) over the entire pattern. The best electron diffraction patterns that we have recorded from bacteriohodopsin with a tapered fibre optics detector have measurable reflections at resolutions of ~ 2 Å. An example of a high-resolution diffraction pattern is shown in Fig. 7(*a*). All diffraction spots in the pattern can be easily identified (Fig. 7(*b*)), and the intensities extracted for further analysis. To compare the performance of the CCD detector with film, a series of diffraction patterns like the ones shown in Fig. 7 were recorded from the same specimen on either the CCD detector or on photographic film under identical electron optical conditions. The intensities in the diffraction pattern were then compiled and analyzed to obtain values for *R*-factors, which report on the overall differences between symmetry related reflections (see Table 1; see also Faruqi *et al*. 1999). The table shows that for resolutions below 5 Å, similar *R*-factors are obtained with data recorded on film or CCD. However, at higher resolutions, as the reflections get weaker and the performance of the CCD detector is measurably superior to that of the film.

Electron diffraction patterns recorded with CCD detectors have been extensively used in structural analysis of bacteriohodopsin (Lindahl & Henderson, 1997; Bullough & Henderson, 1999; Subramaniam *et al*. 1997, 1999; Mitsuoka *et al*. 1999) and in the structure determination of atomic models for the light harvesting complex (Kuhlbrandt *et al*. 1994) and tubulin (Nogales *et al*. 1998).

4. Prospects for high-resolution imaging with CCD detectors

Recording high-resolution images using CCD detectors is obviously a far more challenging prospect than recording electron diffraction patterns. Some of the requirements such as being able to correct for distortions introduced by tapered fibre optics are exactly the same as for recording electron diffraction patterns. Indeed, a few reports (Sherman *et al*. 1996; Downing & Hendrickson, 1999) have already appeared suggesting the feasibility of recording useful high-resolution images from two-dimensional protein crystals. However, the general question of how realistic it is to replace film by CCD detection has not been fully explored. For the purposes of this review, we consider three separate aspects of this question. (1) Are there limitations inherent in camera design such as pixel size which are incompatible with recording images at high resolution? (2) Is the electron dosage required compatible with the low dose requirements of radiation-sensitive biological specimens? (3) Are the areas imaged in a single exposure large enough to be practical for routine imaging work? Below, we address each of these issues in turn.

Because each electron that arrives at the detector contributes to the final image, we first define conditions that allow near-independent pixels to be obtained in the image. For a standard CCD camera with 1:1 coupling between the phosphor and the CCD pixels, 22·5 μm size pixels and a point spread of ~ 120 μm in the phosphor plane, it would take an area that is about five pixels on edge to 'independently' detect a single electron. The effective number of near-independent image pixels that one could get with a $2\,\mathrm{K} \times 2\,\mathrm{K}$ CCD camera would therefore be $\sim 400 \times 400$ pixels. The highest resolution that can be achieved in the detector plane would correspond to the frequency for sampling at one-half of the frequency of independent pixels, which is $\sim 1/(2 \times (5 \times 22{\cdot}5))$, or $1/225\ \mu\mathrm{m}^{-1}$. The resolution that this

https://doi.org/10.1017/S0033583500003577 Published online by Cambridge University Press

https://doi.org/10.1017/S0033583500003577 Published online by Cambridge University Press

Table 1. R-*factors in different resolution ranges*

(1) Film

	p506		p512		p514		p515		p516	
Resolution zone (Å^{-1})	No. of reflections	*R-factor*	No. of reflections	*R*-factor	No. of reflections	*R*-factor	No. of reflections	*R*-factor	No. of reflections	*R*-factor
6·12	126	0·068	126	0·065	123	0·067	126	0·074	126	0·067
4·33	140	0·200	140	0·157	141	0·188	140	0·143	145	0·164
3·53	142	0·170	142	0·175	135	0·158	142	0·205	134	0·191
3·06	144	0·351	79	0·367	48	0·292	117	0·357	103	0·350
2·74	136	0·629	—	—	—	—	23	0·622	5	0·565
2·50	49	0·82	—	—	—	—	—	—	—	—
Overall values	733	0·143	487	0·110	447	0·115	548	0·123	513	0·116

(2) CCD

	s726		s727		s728		s729		s730	
Resolution zone (Å^{-1})	No. of reflections	*R*-factor	No. of reflections	*R*-factor	No. of reflections	*R*-factor	No. of reflections	*R*-factor	No. of reflections	*R*-factor
6·12	109	0·060	104	0·062	105	0·067	111	0·068	103	0·068
4·33	126	0·151	129	0·159	129	0·163	126	0·134	128	0·171
3·53	132	0·160	130	0·186	135	0·157	134	0·149	131	0·150
3·06	140	0·286	138	0·263	131	0·265	127	0·217	138	0·254
2·73	123	0·451	123	0·352	129	0·318	133	0·318	126	0·387
2·50	54	0·505	50	0·479	53	0·464	55	0·428	50	0·438
Overall values	684	0·119	674	0·127	682	0·127	686	0·114	684	0·128

frequency corresponds to in the specimen plane depends on the magnification used. For example, at a magnification of 100 000 ×, 1 Å in the specimen plane corresponds to 10 μm in the detector plane, and the maximum resolution attainable would be 1/22·5 $Å^{-1}$. Note that under these conditions, the spacing on the specimen plane that corresponds to the width of the point spread function is ∼ 12 Å. The total specimen area that could be imaged by the CCD camera would be $(22{\cdot}5 \times 2000\ \mu m)^2$ on the phosphor plane, which corresponds to $(4500\ Å)^2$ in the specimen plane.

The above analysis shows that a square area about 0·5 μm on edge can be imaged with a 2 K × 2 K CCD camera at a magnification of 100 000 × and a resolution of about 22·5 Å. One way to improve the resolution attained would be to use higher magnifications. At 300 000 ×, the resolution improves to 7·5 Å. The improvement in resolution comes, however, at the expense of a reduction in the area images on the specimen, which is reduced to being ∼ 1500 Å wide. Tapered fibre optic coupling provides an excellent approach to improve the resolution without sacrificing the area that is imaged. With a 1·7 taper, only 3 × 3 pixels need to be binned to achieve near-independent pixels, thus, at a magnification of 300 000 ×, the sampling resolution improves to 4·5 Å. With a 2·5 taper, only 2 × 2 pixels need to be binned to achieve near-independent pixels, and the resolution that is attainable increases to ∼ 3 Å. Thus, at 300 000 ×, with a 2·5 fibre optics taper, it should be possible to record images to near atomic resolution from an area that is 0·15 μm × 0·15 μm across.

Next, we consider the electron dosage that would be required to record images with a sufficiently high signal-to-noise ratio, by calculating the dose required to generate an accumulated signal of ∼ 1000 hole pairs per CCD pixel. This value for the signal is almost two orders of magnitude above the expected noise level (see section on noise analysis), and is therefore a conservative value. For the P43 phosphor, we have estimated a value of about 180 electron–hole pairs created for each electron incident on the phosphor for a 1 : 1 taper. Thus, at 100 000 × magnification, for a camera with a standard 1 : 1 taper, with 25 pixels binned, the total required signal would be 25 000 hole pairs (= 139 electrons) for an area that is 112·5 μm × 112·5 μm on the phosphor plane, i.e. 11·25 Å × 11·25 Å wide in the specimen plane, giving an average dose of 1·1 electrons/$Å^2$.

The presence of a taper in the fibre has no effect on the dosage required. With a taper of 2·5, only 2 × 2 pixels need to be binned to get near independent signals, i.e. the area covered by the binned pixels is $\sim 1/(2{\cdot}5)^2$ of the corresponding area on the phosphor plane. As the area imaged on the specimen increases by the same proportion, there is no change in electron dosage. However, there is a 2·5-fold improvement in the resolution limit imposed by the CCD pixel size when compared to the use of 1 : 1 coupling. Because the choice of taper does not influence the electron dose required, the taper can be increased to the point where the improvement in resolution matches the limiting resolution that can be achieved based on the point spread function of the phosphor.

As noted above, the effective resolution that can be attained increases at higher magnifications; however, the corresponding electron dose is also increased. At 300 000 ×, the electron dose is nine times higher than at 100 000 ×. Thus at 300 000 ×, with a 2·5 fibre optics taper coupled CCD camera, it should be possible to record images with excellent signal-to-noise ratio at a dose of ∼ 10 electrons/$Å^2$. This dose is well within the range that is used at present for high resolution images recorded on film. Table 2 shows electron dose requirements and maximum areas that can be imaged at selected magnifications.

The above analysis suggests that it should be possible to record images at near-atomic

https://doi.org/10.1017/S0033583500003577 Published online by Cambridge University Press

https://doi.org/10.1017/S0033583500003577 Published online by Cambridge University Press

Table 2. *Specimen area imaged and electron dose required for different tapers and different magnifications*

Mag.	PSF width at specimen	Nyquist resolution 1:1 taper 5 × 5 binned (Å^{-1})	Nyquist resolution 1·7:1 taper 3 × 3 binned (Å^{-1})	Nyquist resolution 2·5:1 taper 2 × 2 binned (Å^{-1})	Area imaged for 2 K × 2 K CCD 1:1 taper	Area imaged for 2 K × 2 K CCD 1·7:1 taper	Area imaged for 2 K × 2 K CCD 2·5:1 taper	Dose for all tapers corresponding to 1000 ADU
100000	12 Å	$(22{\cdot}5)^{-1}$	$(13{\cdot}5)^{-1}$	$(9{\cdot}0)^{-1}$	4500 Å × 4500 Å	7650 Å × 7650 Å	1·12 mm × 1·12 mm	1·1 e$^-$/Å^2
200000	6 Å	$(11{\cdot}25)^{-1}$	$(6{\cdot}75)^{-1}$	$(4{\cdot}5)^{-1}$	2250 Å × 2250 Å	3825 Å × 3825 Å	5625 Å × 5625 Å	4·4 e$^-$/Å^2
300000	4 Å	$(7{\cdot}5)^{-1}$	$(4{\cdot}5)^{-1}$	$(3{\cdot}0)^{-1}$	1500 Å × 1500 Å	2550 Å × 2550 Å	3750 Å × 3750 Å	9·9 e$^-$/Å^2
400000	3 Å	$(5{\cdot}63)^{-1}$	$(3{\cdot}38)^{-1}$	$(2{\cdot}25)^{-1}$	1125 Å × 1125 Å	1913 Å × 1913 Å	2813 Å × 2813 Å	17·5 e$^-$/Å^2

Above calculations are for operation at 120 kV, assuming PSF of 120 μm at the 1–2% transmission level, 22·5 μm pixels, 1000 ADU counts/pixel corresponding to 16 electrons incident on phosphor.

https://doi.org/10.1017/S0033583500003577 Published online by Cambridge University Press

Table 3. *Estimate of number of molecules that can be imaged for different tapers and magnifications*

Mag.	Number of molecules imaged for 2D crystalline specimen 1:1 taper	Number of molecules imaged for 2D crystalline specimen 1·7:1 taper	Number of molecules imaged for 2D crystalline specimen 2·5:1 taper	Number of molecules imaged for 250 Å wide single particle specimen 1:1 taper		Number of molecules imaged for 250 Å wide single particle specimen 1·7:1 taper		Number of molecules imaged for 250 Å wide single particle specimen 2·5:1 taper	
				Single	16 set	Single	16 set	Single	16 set
100000	2×10^4	$5{\cdot}9 \times 10^4$	$1{\cdot}3 \times 10^5$	81	1296	234	3744	506	8096
200000	5×10^3	$1{\cdot}5 \times 10^4$	$3{\cdot}2 \times 10^4$	20	320	59	944	127	2032
300000	$2{\cdot}3 \times 10^3$	$6{\cdot}5 \times 10^3$	$1{\cdot}4 \times 10^4$	9	144	26	416	56	896
400000	$1{\cdot}3 \times 10^3$	$3{\cdot}7 \times 10^3$	$7{\cdot}9 \times 10^3$	5	80	15	240	32	512

The following assumptions have been used.
There is an average area of 1000 $Å^2$/molecule for two-dimensional crystal.
For single particle, assume that particles are packed at 25% the density of close packed spheres. Thus for 4500 Å edge, can pack 18 molecules × 18 molecules = 324, divide by 4 for 25% density = 81 molecules.

resolution by effectively using fibre optic coupled CCD detectors. However, for practical implementation, it is crucial to consider whether the specimen areas imaged are large enough to allow routine implementation. From inspection of Table 2, it can be seen that at 300000×, with a 2·5 taper, the specimen area that is imaged is only about 3750 Å × 3750 Å, which does not compare favourably with a film image. Thus, although a film image recorded at the same magnification would only correspond to a specimen area of about 2000 Å × 3000 Å, under the usual magnification conditions of 40000× to 60000×, a much larger area could be imaged on film. For effective use of CCD detectors in automated data collection, it is therefore necessary to be able to image larger areas. This is especially important for applications in single molecule microscopy, in which molecules are located in films of ice spread over holes that are ~ 1–2 μm wide.

One approach to imaging larger areas is to adapt spot-scan imaging methods (Bullough & Henderson, 1987; Downing, 1991; Tews, 1996) to create a composite image from several adjacent areas. In currently implemented versions of spot-scan imaging, the beam is deflected in small steps over a specified area of the specimen, resulting in a grid of small images that make up the overall image. Introducing an additional deflection that is applied to the beam before it reaches the image plane, it will be possible to sequentially image each spot to the CCD detector. Sherman *et al*. (1996) have reported implementation of such a scheme to record spot-scan images from crystals of bacteriohodopsin and crotoxin. A simple implementation would involve binning 4 × 4 images, each image taking ~ 20 s for exposure and readout, increasing the area imaged by a factor of 16 without a significant increase in readout noise.

Table 3 shows a calculation of numbers of molecules (crystalline and non-crystalline specimens) that can be imaged at different magnifications using CCD cameras equipped with different tapers. The table allows a quantitative assessment of how changing the taper in the fibre optic assembly, and the use of spot scan imaging can increase the area of the specimen that can be imaged. In a high-quality, low-dose micrograph at 60000× magnification of a single molecule specimen of ~ 250 Å diameter, there are likely to be ~ 1000 useful single particle images. Our conclusion from the above analysis is that by combining a sufficiently high taper (2·5-fold demagnification) with a sufficiently large camera (2 K × 2 K), and by implementing spot scan imaging to bin a small number (16) of images, the CCD camera can provide an equally good if not better alternative to photographic film both in terms of resolution and numbers of molecules imaged.

5. Alternative technologies for electronic detection

5.1 Image plates

Imaging plates were developed originally for use in diagnostic radiography and subsequently used very successfully in lower-energy X-ray crystallographic data collection (Miyahara *et al*. 1986). Compared with film, image plates have higher sensitivity, much larger dynamic range and can be readily digitised. Image plates are sensitive to electrons as well as X-rays and a number of electron applications have been reported recently (Burmeister *et al*. 1994; Zuo *et al*. 1996; Mori, 1998). As with CCD-based detectors, the main component of the image plate is a phosphor, which converts incident radiation (electrons or X-rays) into light. The most commonly used phosphor consists of fine grains of barium fluoro-bromide with small

https://doi.org/10.1017/S0033583500003577 Published online by Cambridge University Press

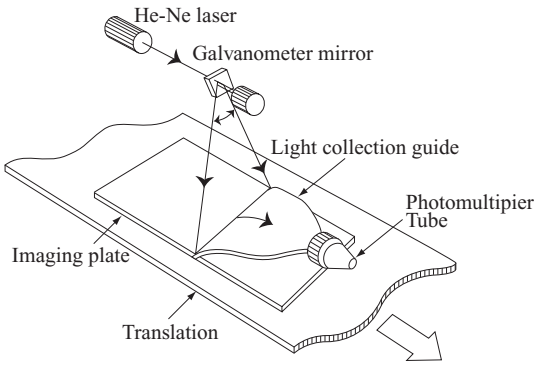


Fig. 8. Schematic layout of an image plate readout system (adapted from Miyahara *et al*. 1996). The He–Ne laser provides the laser beam for reading the plate and the beam is scanned across the plate by a rotating mirror mounted on a deflection coil. The plate is moved in the orthogonal direction, the emitted light being collected by a suitable light guide and recorded by a photomultiplier. Several different types of readout have been devised more recently, but the essential principle is the same.

amounts of europium ($BaFBr:Eu^{2+}$). The phosphor is usually deposited in a layer of 50–100 μm thickness on to a plastic 'backing' plate for rigidity. In contrast to phosphors such as P43, where the conversion of electron energy to light occurs within milliseconds, the image plate phosphor is excited into a metastable state following photon or electron absorption. Illumination of the phosphor with a secondary beam of visible light (usually from a He–Ne laser at 633 nm) triggers recovery of the ground state, a process which results in the emission of photons with a wavelength of 390 nm. The schematic diagram showing the essential features of an image plate readout system is shown in Fig. 8 (Miyahara *et al*. 1986). The number of photons emitted by the image plate phosphor are proportional to the absorbed energy, providing a detector that has excellent linearity covering a 10000-fold range in the intensity of incident radiation. The light photons are detected by a sensitive photomultiplier, digitized and stored.

An image plate thus acts essentially like a re-usable 'film' on which the pattern is recorded and then removed for scanning in a special reader before being re-used for further exposures. The resolution attained, in terms of MTF at the Nyquist frequency, is typically $\sim 0{\cdot}4$, reported by Zuo *et al*. (1986), using a standard film-sized image plate with 25 μm pixels. It is better than film in terms of dynamic range, and does not suffer from background 'fog' because the image plate can be cleared of any accumulated noise 'signal' prior to each exposure; this is useful for detecting low-level signals. The main disadvantage of image plates is that, like film, they are not on-line devices so one needs to remove the IP from the camera vacuum and scan it before any results are available to the user.

5.2 Hybrid pixel detectors

As discussed earlier, silicon can be used as a direct imaging material, made possible by converting the incident electron or X-ray energy into electron–hole pairs. Provided a suitable potential is applied to the silicon, the electrons can be detected on an electrode. This method is used in X-ray astronomy for recording low-flux X-ray images directly in CCD detectors. The term hybrid pixel detectors is applied to two-dimensional detectors, usually but not

https://doi.org/10.1017/S0033583500003577 Published online by Cambridge University Press

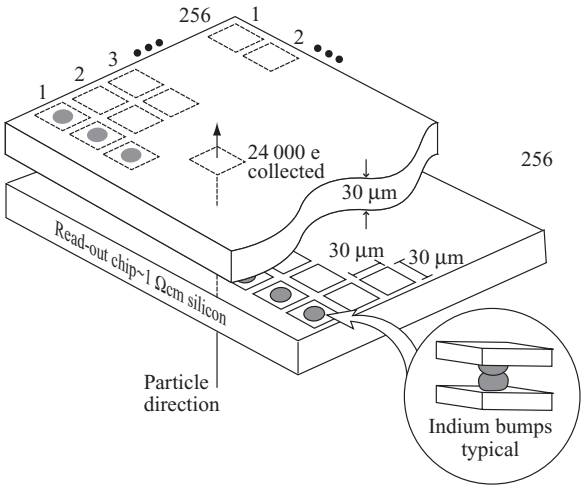


Fig. 9. Schematic diagram of an early version of a hybrid pixel detector, intended for a particle physics application, adapted from Shapiro *et al*. (1989). The detector and readout electronics pixels are coupled by a bump-bond. Electrons (or holes) generated in the detector are collected by the readout amplifier which generates a single count per event.

exclusively based on silicon, in which the detecting elements are arranged in an array (Heijne, 1988; Shapiro *et al*. 1989; Hall, 1995). In a silicon pixel detector (Fig. 9, adapted from Shapiro *et al*. 1989), silicon is divided up into a number of discrete pixels on one chip, and bonded to readout electronics on a separate chip. The main difference between the readout of CCD detectors and silicon pixel detectors is that in the former, analog charge from individual pixels is transferred into one or two output amplifiers for digitization. In the latter, readout is purely digital, with each pixel having its own readout channel which counts the number of 'hits' in a local scaler.

Silicon pixel detectors, which were originally proposed for imaging infra-red radiation and subsequently adapted to particle physics and medical radiography (Schwarz *et al*. 1999), offer a direct detection alternative to CCD detectors, i.e. without converting the energy of the incident electron into light first. The basic concept of the hybrid pixel detector is quite simple: the detector and readout electronics are produced on two separate wafers, the front wafer containing the detector elements, which are essentially biased diodes, etched on a high-resistivity substrate using photolithography, and bonded to the readout electronics on a similar array based on low-resistivity silicon. Charge generated by an incoming electron is swept by the electric field on to an electrode where it is 'sensed' by the amplifier on the readout chip. The small pixel size ensures low noise, i.e. high rate operation. The single channel electronics consists of an amplifier, discriminator and a scaler. Incident electrons produce a voltage pulse which is amplified and if it exceeds a threshold set in the discriminator, increments the scaler count by one. The operation of the pixel detector is thus almost entirely digital. The advantage of the 'hybrid' concept is that one can substitute different detector materials, e.g. gallium arsenide, cadmium telluride for silicon in experimental situations where a high-Z material is required, but use a similar readout electronics chip.

The main advantage of pixel detectors is the potential for better spatial resolution than can be obtained with CCD based detectors and, ultimately, a larger number of independent pixels,

https://doi.org/10.1017/S0033583500003577 Published online by Cambridge University Press

with much faster readout times. Because the detectors are digital, the dynamic range is determined by the size of the memory storage rather than the size of the pixel well capacity as for CCD detectors. Additionally, as pointed out by Fan *et al*. (1998), who have tested an 8×8 pixel detector designed originally for protein crystallography, the problems associated with X-ray induced noise signals should be less troublesome as they can only register as a single count. It was found that charge sharing between adjacent pixels (which were 150 μm^2) only became significant above $\sim$ 200 keV owing to the larger spread in generated charge by the incident electron, as predicted by Monte Carlo simulations. It may be possible to reduce this effect by using a higher density and Z material, e.g. GaAs or Cd(Zn)Te as the detector, but more experience is needed before these materials can be used with the same confidence as silicon.

6. References

Autrata, R., Schauer, P., Kvapil, J. & Kvapil, J. (1983). Single-crystal aluminates – a new generation of scintillators for scanning electron microscopes and transparent screens in electron optical devices. *Scanning Electron Microscopy* **11**, 489–500.

Baldwin, J. & Henderson, R. (1984). Measurement and evaluation of electron diffraction patterns from two-dimensional crystals. *Ultramicroscopy* **14**, 319–336.

Baumeister, W. (1999). Electron tomography of molecules and cells. *Trends Cell Biology* **9**, 81–85.

Brink, J. & Tam, M. W. (1996). Processing of electron diffraction patterns acquired on a slow-scan CCD camera. *J. struct. Biol.* **116**, 144–149.

Bullough, P. A. & Henderson, R. (1987). Use of spot-scan procedure for recording low-dose micrographs of beam-sensitive specimen. *Ultramicroscopy* **21**, 223–230.

Bullough, P. A. & Henderson, R. (1999). Projection structure of the K intermediate of the bacteriorhodopsin photocycle determined by electron diffraction. *J. molec. Biol.* **286**, 1663–1671.

Burmeister, C., Braun, H. G. & Schroder, R. R. (1994). A new quasi-confocal image plate scanner with improved spatial resolution and ideal detection efficiency. *Ultramicroscopy* **55**, 55–65.

Coleman, C. I. (1985). Imaging characteristics of rigid coherent fibre optic tapers. In *Advances in Electronics and Electron Physics* **64**B, 649–661. Academic Press.

Daberkow, I., Hermann, K.-H., Liu, L. & Rau, W. D. (1991). Performance of electron image converters with YAG single crystal screen and CCD sensor. *Ultramicroscopy* **38**, 215–223.

Daberkow, I., Hermann, K.-H., Liu, L., Rau, W. D. & Tietz, H. (1996). Development and performance of a fast fibre-plate coupled CCD camera at medium energy and image processing system for electron holography. *Ultramicroscopy* **64**, 35–48.

de Ruijter, W. J. & Weiss, J. K. (1992). Methods to measure properties of slow-scan CCD cameras for electron detection. *Rev. scient. Instrum.* **63**, 4314–4321.

Downing, K. H. (1991). Spot-scan imaging in transmission electron microscopy. *Science* **251**, 53–59.

Downing, K. H. & Hendrickson, F. M. (1999). Performance of a 2 K CCD camera designed for electron crystallography at 400 kV. *Ultramicroscopy* **75**, 215–234.

Fan, G. Y., Datte, P., Beuville, E., Beche, J.-F., Millaud, J.-F., Downing, K. H., Burkaard, F. T., Ellisman, M. H. & Xuong, N.-H. (1998). ASIC-based event-driven 2D digital electron counter for TEM imaging. *Ultramicroscopy*, **70**, 107–113.

Fan, G. Y. & Ellisman, M. H. (1993). High-sensitivity lens-coupled slow-scan CCD camera for transmission electron microscopy. *Ultramicroscopy* **52**, 21–29.

Fan, G. Y. & Ellisman, M. H. (1997). Optimisation of thin-foil based phosphor screens for CCD imaging in TEM in the voltage range 80–400 kV. *Ultramicroscopy* **66**, 11–19.

Faruqi, A. R. (1991). Applications in biology and condensed matter physics. *Nucl. Instrum. Meth.* A**310**, 14–23.

Faruqi, A. R. & Andrews, H. N. (1997). Cooled CCD camera with tapered fibre optics for electron microscopy. *Nucl. Instrum. Meth.* A**392**, 233–236.

Faruqi, A. R., Andrews, H. N., Cattermole, D. C. & Stubbings, S. (2000). A tiled CCD detector with 2 by 2 array and tapered fibre optics for electron microscopy. *Nucl. Instrum. Meth.* (in press).

Faruqi, A. R., Andrews, H. N. & Henderson, R. (1995). A high sensitivity imaging detector for electron microscopy. *Nucl. Instrum. Meth.* A**367**, 408–412.

Faruqi, A. R., Andrews, H. N. & Raeburn, C. (1994). A large area cooled-CCD detector for electron microscopy. *Nucl. Instrum. Meth.* A**348**, 659–663.

https://doi.org/10.1017/S0033583500003577 Published online by Cambridge University Press

Faruqi, A. R., Henderson, R. & Subramaniam, S. (1999). Cooled CCD detector with tapered fibre optics for recording electron diffraction patterns. *Ultramicroscopy* **75**, 235–250.

Faruqi, A. R. & Tyrell, G. C. (1999). Evaluation of gadolinium oxy-sulphide (P43) phosphor used in CCD detectors for electron microscopy. *Ultramicroscopy* **76**, 69–75.

Hall, G. (1995). Silicon pixel detectors. *Q. Rev. Biophys.* **28**, 1–32.

Heijne, E. H. M., Jarron, P., Olsen, A. & Redaelli, N. (1988). The silicon micropattern detector: a dream? *Nucl. Instrum. Meth.* A**273**, 615–619.

Krivanek, O. L. & Mooney, P. E. (1993). Applications of slow-scan CCD cameras in transmission electron microscopy. *Ultramicroscopy* **49**, 95–108.

Kuhlbrandt, W., Wang, D. N. & Fujiyoshi, Y. (1994). Atomic model of plant light-harvesting complex by electron crystallography. *Nature* **367**, 614–621.

Kujawa, K. & Krahl, D. (1992). Performance of a low-noise CCD camera adapted to a transmission electron microscope. *Ultramicroscopy* **46**, 395–403.

Lindahl, M. & Henderson, R. (1997). Structure of the bacteriorhodopsin D85N/D96N double mutant showing substantial structural changes and a highly disordered, twinned lattice. *Ultramicroscopy* **70**, 95–106.

McLean, I. S. (1989). *Electronic and Computer-Aided Astronomy*. John Wiley & Sons.

Meyer, R. R. & Kirkland, A. (1998). The effects of electron and photon scattering on signal and noise transfer properties of scintillators in CCD cameras used for electron detection. *Ultramicroscopy* **75**, 23–33.

Mitsuoka, K., Hirai, T., Murata, K., Miyazawa, A., Kidera, A., Kimura, Y. & Fujiyoshi, Y. (1999). The structure of bacteriorhodopsin at 3·0 Å resolution based on electron crystallography: implication of the charge distribution. *J. molec. Biol.* **286**, 861–882.

Miyahara, J., Takahashi, K., Amemiya, Y., Kamiya, N. & Satow, Y. (1986). A new type of X-ray area detector utilizing laser stimulated luminescence. *Nucl. Instrum. Meth.* A**246**, 572–578.

Mori, N. (1998). The imaging plate and its applications. In *Advances in Imaging and Electron Physics* **99**, 241–290. Academic Press.

Nogales, E., Wolf, S. G. & Downing, K. H. (1998). Structure of the alphabeta tubulin dimer by electron crystallography. *Nature* **391**, 199–203.

Roberts, P. T. E., Chapman, J. N. & MacLeod, A. M. (1982). A CCD-based recording system for CTEM. *Ultramicroscopy* **8**, 385–396.

Schwarz, C., Campbell, M., Goeppert, R., Heijne, E. H. M., Ludwig, J., Meddeler, G., Mikulec, B., Pernigotti, E., Rogalla, M., Runge, K., Soeldner-Rembold, A., Smith, K. M., Snoeys, W. & Watt, J. (1999). X-ray imaging using a hybrid photon counting GaAs pixel detector. *Nucl. Phys. B, Proc. Suppl.* **78**, 491–496.

Shapiro, S., Dunwoodie, W., Arens, J., Gernigan, J. & Gaalema, S. (1989). Silicon PIN diode array hybrids for charged particle detection. *Nucl. Instrum. Meth.* A**275**, 580–586.

Sherman, B. S., Brink, J. & Chiu, W. (1996). Performance of a slow-scan CCD camera for macromolecular imaging in a 400 kV electron cryomicroscope. *Micron* **27**, 129–139.

Subramaniam, S., Faruqi, A. R., Oesterhelt, D. & Henderson, R. (1997). Electron diffraction studies of light-induced conformational changes in the Leu-93 Ala bacteriorhodopsin mutant. *Proc. natn Acad. Sci. USA* **94**, 1767–1772.

Subramaniam, S., Lindahl, M., Bullough, P., Faruqi, A. R., Tittor, J., Oesterhelt, D., Brown, L., Lanyi, J. & Henderson, R. (1999). Protein conformational changes in the bacteriorhodopsin photocycle. *J. molec. Biol.* **287**(1), 145–161.

Tews, I. (1996). Ph.D. Thesis, University of Heidelberg, Germany.

Zuo, J. M., McCartney, M. R. & Spence, J. C. H. (1996). Performance of imaging plates for electron recording. *Ultramicroscopy* **66**, 35–47.

https://doi.org/10.1017/S0033583500003577 Published online by Cambridge University Press